

MEMS-on-CMOS integration of a holographic 8M-Pixel SLM device using KrF-Lithography

S. Döring*, P. A. Recknagel, C. Hohle, P. Dürr

Fraunhofer Institute for Photonic Microsystems IPMS, Maria-Reiche-Str. 2, D-01109 Dresden, Germany

ABSTRACT

We discuss the process integration to manufacture a spatial light modulator (SLM) device for application in mixed and augmented reality. The MEMS-part of the device is integrated on an external 180nm CMOS. The SLM consists of an 8MPixel micro mirror array with a pixel size of $4\mu\text{m} \times 6\mu\text{m}$. To provide the vertical strokes necessary for RGB color image generation, a comb-drive actuator concept was developed. Besides the yoke and the stator of the comb-drive, the actuator uses a double spring structure to reduce tilting of the mirror and other stress-induced effects. At the beginning of the product development we used iLine-lithography only, while later for the final device we switched to KrF-lithography to provide the necessary feature size down to 200nm as well as better CD-uniformity and overlay specification. We describe the process development, with focus on the lithography and etching processes for the actuator. Especially the different processes for patterning the Titanium-Aluminum structures of ultra-thin springs as well as the yoke and the stator with their high aspect ratios, which are specific for MEMS processing. Finally we achieved post-etch CD-uniformity $<10\text{nm}$ per wafer for all metal structures as well on-product-overlay accuracy $<15\text{nm}$.

Keywords: Spatial Light Modulator, SLM, MMA, AR/MR/VR, integration, holography, MEMS, KrF-Lithography

1. INTRODUCTION

In the last decade there has been a growing interest in augmented, mixed and virtual reality applications. However commercially available stereoscopic and volumetric displays suffer from specific drawbacks, which diminish the user experience. A pathway to real-time realistic 3D holographic displays using Computer-Generated-Holography (CGH) was proposed 15 years ago [1]. In CGH a fringe pattern is calculated and transferred to a spatial light modulator (SLM), which diffracts the light in a specific manner, that for the user the desired image is created in far field. An SLM, which is suitable for holographic application needs to provide a precise multilevel phase control of coherent light with sufficient precision and high frame rates. Commercial SLMs already available are often Liquid Crystal on Silicon (LCoS) devices [2]. In the REALHOLO project [3], funded within the EU Framework program Horizon 2020, we take another approach by using a Micro-Mirror-Array (MMA), which offers the potential for significantly better performance than LCoS. The MMA developed for this project here is based on a comb-drive actuator concept, using 8 million phase-shifting pixels of $4 \times 6\mu\text{m}^2$ size. There are already publications about this design and simulation of this device [4-6] as well as first results on characterization of passive devices using such comb-drive [7,8].

In the current work we do not focus on the device, but the process integration on which it is based. Within this Horizon project the Fraunhofer IPMS is responsible for the preparation of the MMA. The full MEMS-part is integrated on top of CMOS-wafers provided by the project partner X-FAB, which are fabricated in 180nm technology node. At the project start, our clean room could only make use of iLine lithography in form of a Nikon NSR-2205i14E2 5:1 stepper. While this tool is good enough for standard MMAs with larger pixel size of $16\mu\text{m}$ and above, it restricted the first designs with respect to applicable CD feature sizes and overlay. In 2022 we did an important upgrade of our lithography section by purchasing a Nikon NSR-S210D 4:1 KrF-scanner [9]. While such tool still can be labeled as mature with respect to cutting edge technologies in memory and logic fabrication, usage of KrF-lithography for MEMS fabrication is not widespread, although previously predicted [10]. This new tool allows more complex layouts of the comb-drive actuator with improved design rules.

*Sebastian.doering@ipms.fraunhofer.de; www.ipms.fraunhofer.de

2. COMB-DRIVE ACTUATOR

The comb-drive actuator consists of 6 metal layers as shown in the cross-sections in Figure 1. The lowest layer is the base plate, like the subsequent layers (spring 1, yoke, stator and spring 2) are made from Titanium-Aluminum, a material commonly used at the IPMS for mechanical elements due to its superior elastic properties [11]. The mirror is made from an Al-alloy for high reflectivity at visible wavelength. All metal layers are deposited using DC-sputtering, whereas the sacrificial layers are deposited by PE-CVD. The PE-CVD is also used for the filled vias underneath the mirror and spring 2, which are made from amorphous silicon. The base plate has via connections to the top metal of the CMOS and additionally acts as light shield protecting the CMOS from scattered light to avoid unwanted charge generation or switching of transistors. Optionally an additional light shield can be integrated between the top metal and the base plate to increase the protection. Since the full actuator uses undoped silica glass (USG) as sacrificial layer, which later within the packing process is released using either hydrogen fluoride gas or CF_4 plasma etching, the insulating layers of the CMOS need protection against the release etchants. This is done by an Al_2O_3 barrier underneath the base plate. During preparation the first via for CMOS connection as well as the base plate itself are less critical layers and iLine-lithography can be used. Thereafter higher precision is required and so the first layer, which uses KrF-lithography is the spring 1 layer. For leading edge technologies, usually feature size and thus the lithography used gets more relaxed with processing progress from (immersion)ArF or even EUV to KrF and further iLine-lithography. Here we have the uncommon situation, that the CMOS processing for 180nm node starts with KrF in the FEoL, switches to iLine in the BEoL, we take over still using iLine-lithography for the first MEMS layers but go back to the more precise KrF-lithography in the later processing. The switch of lithography between an external fab as well as internally from 5:1 stepper to 4:1 scanner sets high requirements for mix-and-match interoperability.

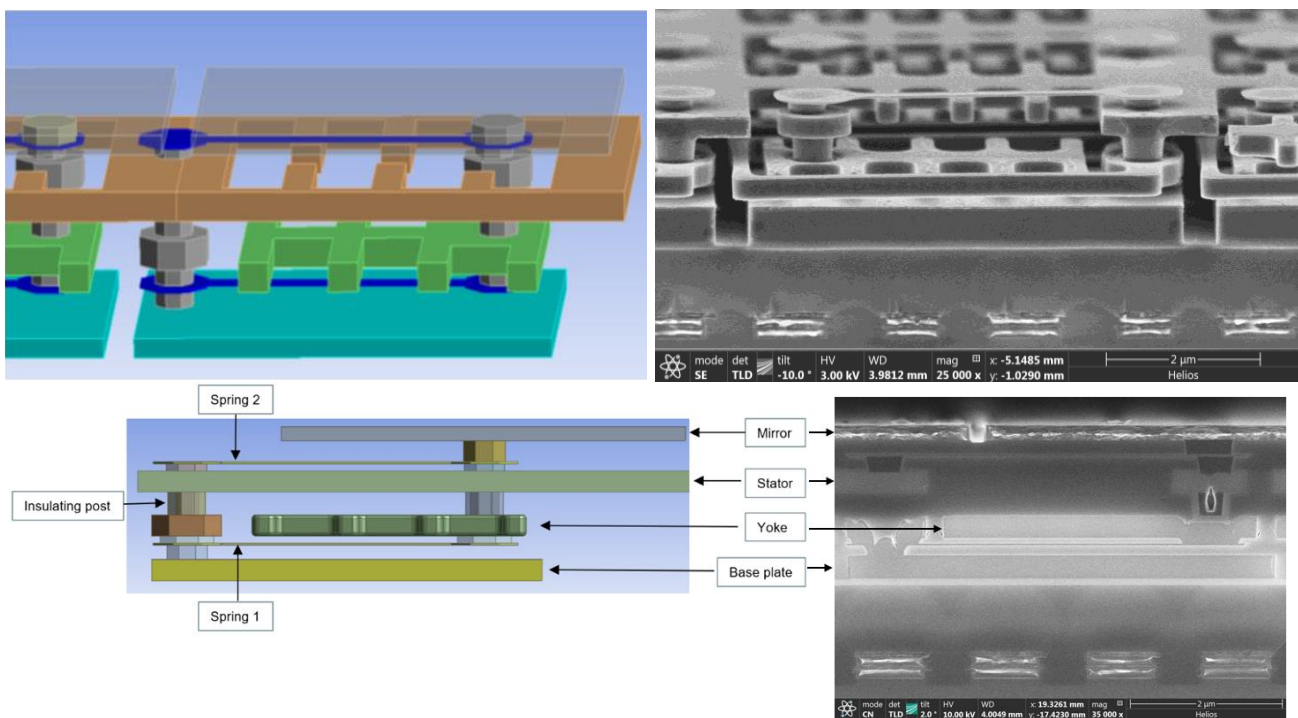


Figure 1: Tilted view (top) and cross-section (bottom) of the comb drive actuator as schematic (left) and SEM-image (right).

The actual design of the comb-drive actuator evolved during process development. As mentioned above, at the beginning we were restricted by iLine-lithography. Therefore, we started with a simple design using a pixel size of $3 \times 6 \mu\text{m}^2$ and only 2 fingers for the comb drive (composed by yoke and stator). The minimum feature-size was 400nm as limit of the technology design rules (Figure 2). This design was trialed on small passive test chips of $6 \times 6 \text{mm}^2$ and several variants of spring layouts were tested. Finally, we decided on straight spring, which can be approximated as isolated lines. However,

it was clear that such design can only act as a prove of concept of the comb-drive but not fulfill the specification of the final device. The next evolution step in the design was the 4-finger comb design applied on large passive test chips. These chips have the same 8MPixels and similar chip size as the final active chip of 21.0 x 19.5 mm². In this 4-finger design the pixel size has been increased to 4 x 6 μm² for a number of reasons but allowed 4 fingers per actuator cell, which generate more electrostatic actuator force. The first version of this chip was still compatible with iLine-lithography, but subsequently the fingers of the comb drive have been shrunken to 340nm CD and minimum tested spring CD was 200nm (Figure 3). The final layout was a 5-finger design using the same 4 x 6 μm² pixel size as the 4-finger design but with the finger CD reduced down to 240 nm. Simulations predicted a higher electro-static force compared to the 4-finger design. Additionally, as shown in Figure 4, it incorporates an additional structure around the fingers to reduce cross-talk to neighbor pixels. Due to the additional finger and the cross-talk-ring, this design has more strict design rules and can only be achieved by using KrF-Lithography. This design will finally be applied on the active CMOS-devices. Theoretically, the scanner specifications would allow further reduction of the finger CD for implementation of a sixth finger, however our simulations showed no benefit on drive sensitivity for such a configuration. An overview of the designs and its parameters is shown in Table 1. A detailed description of the full process flow including non- litho/patterning process like PVD/CVD and CMP processes can be found in [12]. In the next section 3 we will focus on development of single layer lithography and patterning mainly of the critical layers of springs and yoke/stator while later in Section 4 we will discuss results from the full process integration with focus on on-product overlay and CD-uniformity of the final device.

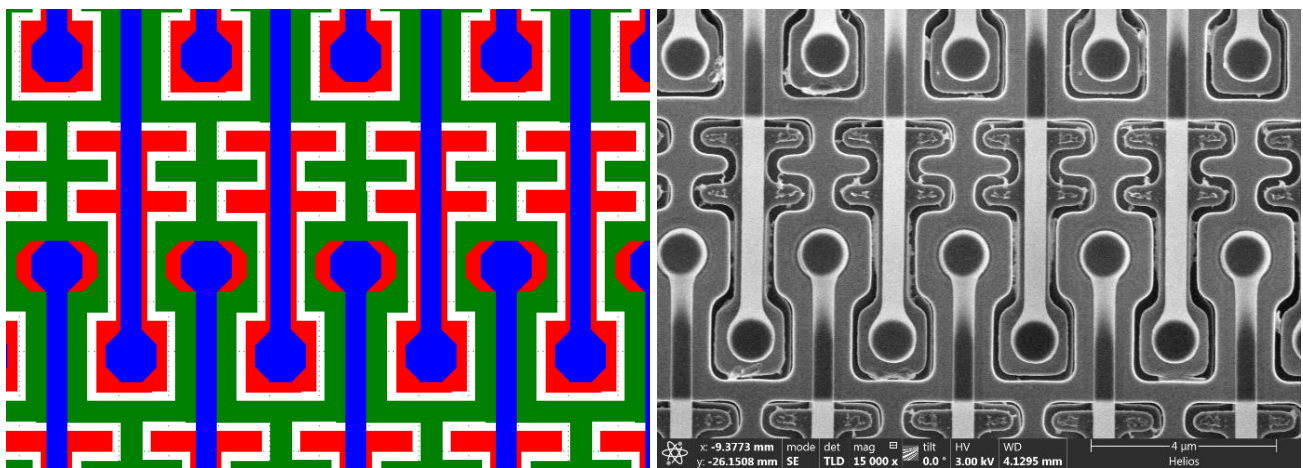


Figure 2: Layout with yoke (red), stator (green) and spring (blue) on the left side and SEM top view of the small passive layout using 6 x 3 μm² cell size.

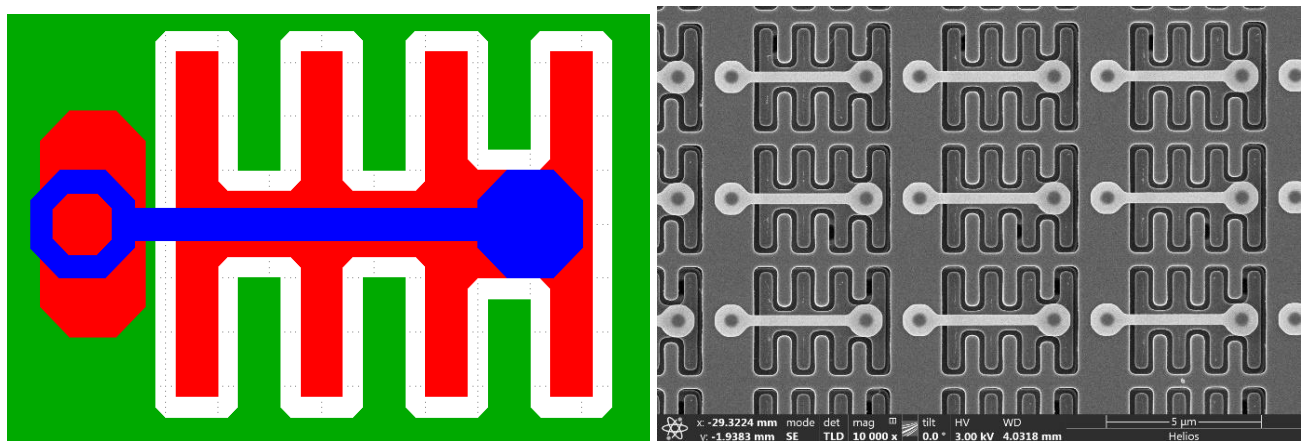


Figure 3: Layout with yoke (red), stator (green) and spring (blue) on the left side and SEM top view of the 4-finger layout using 6 x 4 μm² cell size.

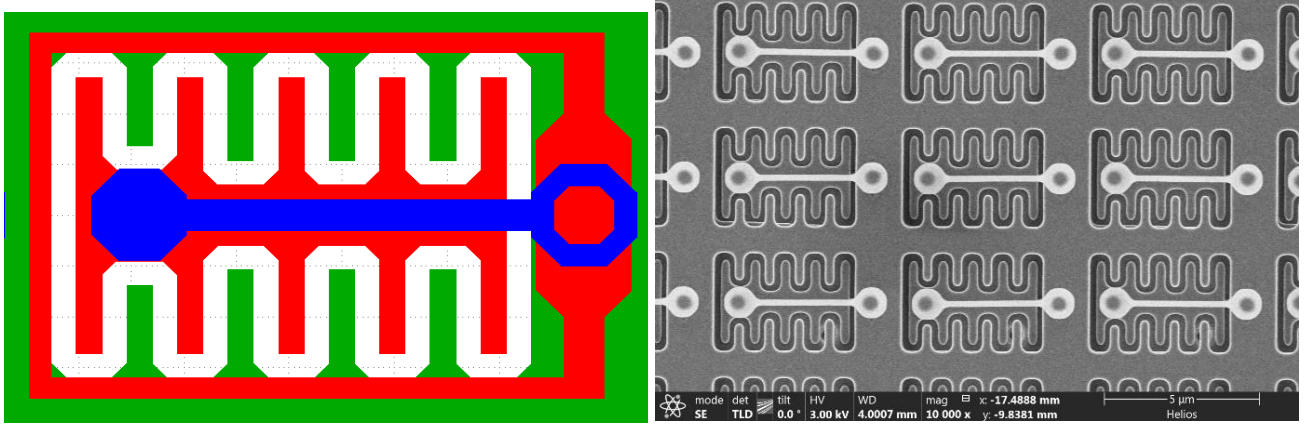


Figure 4: Layout with yoke (red), stator (green) and spring (blue) on the left side and SEM top view of the 5-finger layout using $6 \times 4 \mu\text{m}^2$ cell size.

Table 1. Overview of design variants, lithography used and minimum feature sizes.

Design	Lithography	Minimum CD spring	Minimum CD yoke/stator
Small passive 2 finger	iLine-only	400nm	400nm
Large passive 4 finger	KrF, backwards compatible to iLine	200nm, fallback option to 400nm	340nm, fallback option to 400nm
Large passive 5 finger	KrF-only	200nm	240nm

3. SINGLE LAYER LITHOGRAPHY AND PATTERNING

While development of all layers had their challenges, this work will focus on lithography and patterning of the crucial metal layers only, namely the springs, yoke and stator. The patterning of circular vias, for example, using KrF-lithography (even with the aspect ratio of 1:1 present in our actuator concept) is actually not known as exceptionally challenging even in matured nodes. Furthermore, these structures are less critical with respect of CD-uniformity as well as overlay error. The same applies to the mirror, where a small trench between single pixel and small corner rounding is desired, to provide a high fill grade. However, these types of processes do not push the used tools to their limits.

For iLine-lithography we used a Nikon NSR-2205i14E2 5:1 iLine-stepper and a SCREEN SK-80EX Track in combination with DOW SPR700 resist. For KrF-lithography we used a Nikon NSR-S210D 4:1 KrF-scanner and a TEL Clean Track ACT8. As BARC we used DOW AR10L and the resist was either DOW UV1100 for thin layers like the springs and DOW UV5 for thicker layers like yoke and stator. The patterning of metal structures was done on a LAM TCP 9600 PTX RIE tool.

Springs

The springs are made from TiAl of approximately 30nm thickness. The actual thickness for best device performance is still under evaluation because natural and artificial oxidation during subsequent CVD as well as during the release of the sacrificial layers need to be taken into account. To prevent oxidation as well degradation of the springs Originally different layouts for springs where tested and on the passive devices two candidates remains. The straight springs, which can be labeled as isolated-lines and another design called Q-springs, which comes closer to a lines/space (1:3 ratio) pattern. Both layouts where packed on a single multi-purpose die, incorporating also a CD variation of 200 and 300nm for both layouts.

While the shape of the spring itself is pretty simple and thus, pattern fidelity is not an issue, CD-uniformity i.e. per die needs to be kept close to the possible optimum. Since CD of the springs linearly transfers to stiffness, a CD-variation over the MMA leads to phase variation and thus loss of contrast in the final image. To reduce the effect of resist thickness variation over the wafer and die area, we found the lowest amplitude of the swing curve of only 3nm using a conventional aperture with $iNA=0.328$, compared to other conventional dipole apertures (Figure 5).

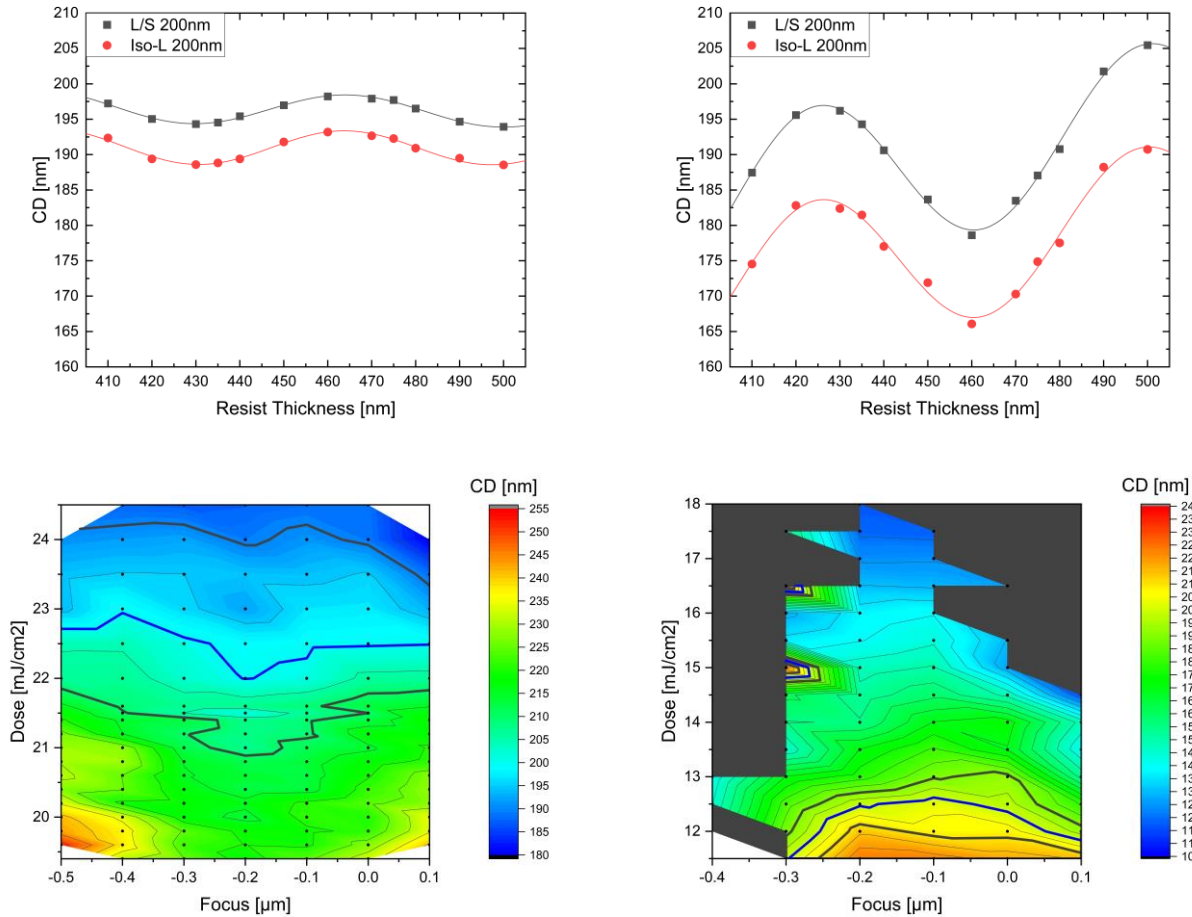


Figure 5: Top: Swing-Curve for 200nm isolated lines (straight springs) in red and L/S (Q-springs) in black using conventional aperture with $iNA=0.328$ (left) and X-dipole with $iNA=0.7$, $RET=0.8$ (right). Bottom: Focus-Exposure-Matrix for 200nm isolated lines (straight springs) using 50nm BARC and 435nm resist for the same apertures as above.

The same parameter settings were then investigated regarding best focus and dose. Again, using a conventional aperture with $iNA=0.328$ leads to a high parameter window at a depth of focus $>0.4\mu m$, as shown in Figure 5. After fixing these optimal parameters of BARC and resist thickness, focus offset and dose, development of the patterning process was started. As etchants for patterning of TiAl structures the reactive ion etch tools use a mixture of Cl_2 and BCl_3 gas. This chemistry is well known for patterning of Al interconnect as well as TiN and Ti layers [13,14], and thus can be optimized for Ti-Al-alloys, too. As a final result of the development, two processes were proven as acceptable for the spring patterning. When using $iNA=0.328$ for litho, both provided a small CD shift from After-Development-Inspection (ADI) to After-Etch-Inspection (AEI) and also only a minimal easing of the CD-uniformity. As shown in Figure 6, a variation within a single wafer for both, the straight as well as the Q-springs of $\pm 10nm$ AEI could be achieved.

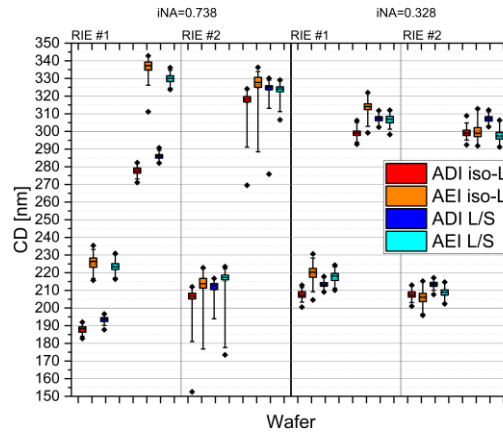


Figure 6: CD-Uniformity per Wafer for 200/300nm isolated lines (straight springs) and L/S (Q-springs) comparing ADI and AEI for two aperture and etch settings.

Yoke and Stator

The yoke and stator are significantly different from springs. While for the springs, pattern fidelity is pretty easy, firstly due to their shape as isolated line and secondly due to the small aspect ratio. The yoke and stator both consist of a 300nm thick TiAl layer, an order of magnitude higher than the springs. Additionally at deposition a sputtered hard mask made from TiN is applied and needs to be patterned, too. The role of this hard mask is to protect the TiAl from physical and chemical cleaning processes applied post-etch. Such cleaning procedures can reduce residues emerging during the release process, residues which probably have their origins in patterning induced contaminations of the sacrificial layer underneath the metal. After these cleaning procedures, the TiN can be removed using O_2/CF_4 plasma. Patterning therefore, needs to pattern a lateral feature size down to 240nm into 340nm thick TiAl/TiN-layer and this with high pattern fidelity of the fingers, to ensure the drive parameters end up close to calculated values. For the 4-finger design this task was still relaxed, as can be seen in Figure 7. By using the full aperture of $iNA=0.738$, which should provide the best pattern fidelity with drawbacks in depth of focus a wide parameter range in focus-exposure-matrix $>0.6\mu m$ can be found and the fingers show a good pattern transfer at slightly negative focus offset, when imaged in SEM.

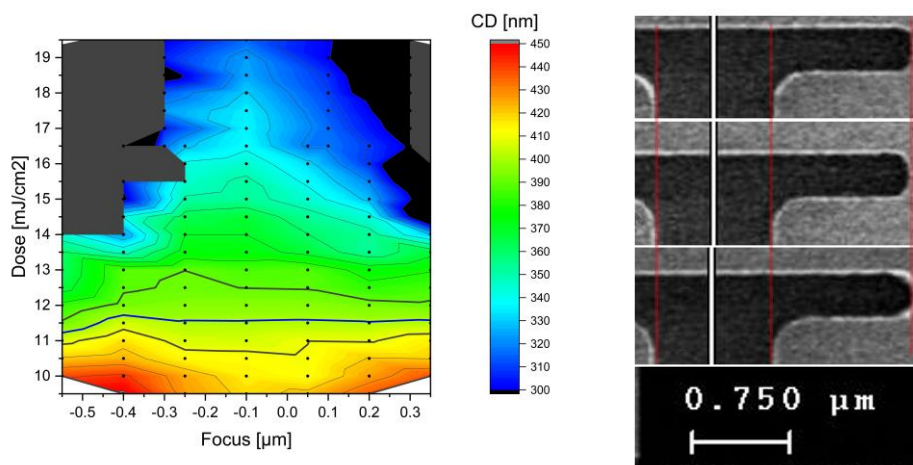


Figure 7: Left-Side: Focus-Exposure-Matrix for a 4-finger yoke (CD=400nm) using 50nm BARC and 775nm resist at $iNA=0.738$. Right side: Images from CDSEM at dose=11.5mJ/cm² and a focus offset of -0.25µm (top), -0.10µm (center) and +0.05µm (bottom).

The situation got more complex for the 5-finger design. Figure 8 shows focus-expose-matrices for three different settings of conventional apertures using $iNA=0.738$, 0.328 and 0.205 for the exposure of the yoke. The process window for the highest iNA got significantly smaller compared to the 4-finger design from Figure 7. Reducing the iNA to 0.328 re-established a wider process window again. SEM images shows that when using the best settings for exposure, corner rounding for smaller fingers gets more crucial (as expected), but generally pattern fidelity still looks acceptable. Since the yoke and stator have a similar shape (for the same overall actuator design) due the necessity of fingers intermeshing with each other, the best exposure parameters are close for both layers. Figure 3 and Figure 4 presented above both already show a good pattern fidelity of both layers not only at single layer patterning but there for released chips after full wafer processing (note, however, for these tests the mirror layer has been skipped for destruction-free analysis).

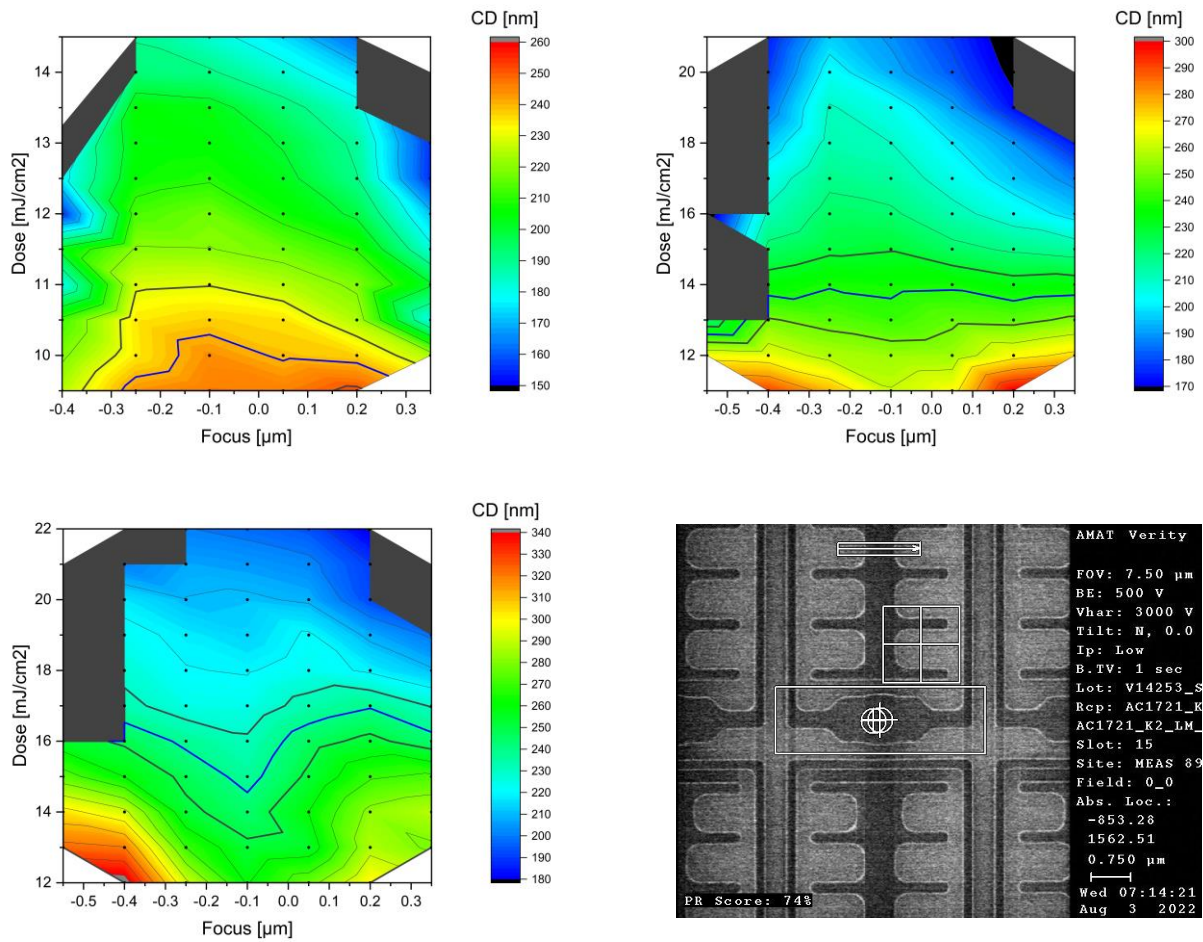


Figure 8: Focus-Exposure-Matrix for a 5-finger yoke (CD=240nm) using 50nm BARC and 775nm resist at $iNA=0.738$ (top left), $iNA=0.328$ (top right) and $iNA=0.205$ (bottom left). The image at bottom right shows an ADI image from CD-SEM at best focus-dose parameters 14mJ/cm^2 , $-0.1\mu\text{m}$ at $iNA=0.328$.

Even with the emphasized attention on pattern fidelity for the yoke and stator as compared to the springs, CD-uniformity is no less important for both, the yoke and the stator. The longer etch time in the RIE makes the process more sensitive to etch-rate uniformity over the wafers, which transfers into CD-variations of patterned structure. Furthermore, these metal structures needs to be filled and planarized by USG. The topology, which remains after CMP, as well as thickness variations can dramatically shrink the process window and the available depth of focus for exposure can be smaller than for simple single layer process development. For wafer processing of the passive devices using the 5-finger design at the

time of writing, 4 lots are already processed or still in preparation. Data from the CD-SEM for these lots for yoke and stator are shown in Figure 9. After overcoming uniformity issues in the very first lot, we could achieve a per-wafer CD-uniformity of <10nm for best lots/wafers. However, process stability still is a work in progress. Especially, the aforementioned post-etch-cleaning procedures can influence the CD-uniformity. This is visible for lot#4 of the yoke patterning, where a different cleaning approach was tested, leading to a worsening of the CD-uniformity from <10nm to ~15nm.

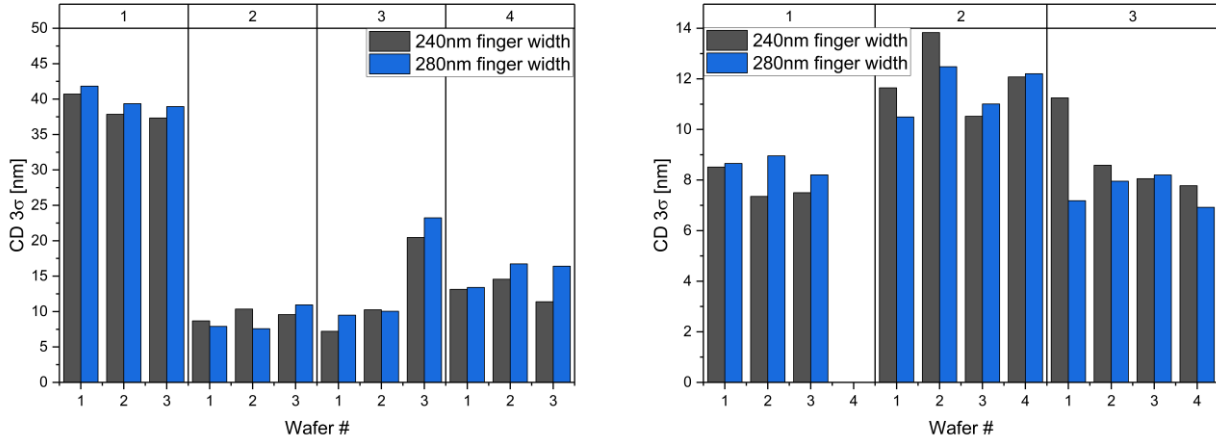


Figure 9: CD-uniformity per wafer for 5-finger yoke (left) and stator (right) for 4, respectively 3 lots. Lot #4 did not reach stator patterning at the time of this work.

4. ON-PRODUCT OVERLAY

Another important parameter for the comb-drive actuator besides CD-uniformity and pattern fidelity is overlay, particularly between stator and yoke. For this parameter, there is a soft specification of 30nm and a hard specification of 15nm. Since both layers are separated by a planarized USG-layer in the product, the alignment of the stator layer cannot be done directly on marks prepared during the yoke patterning, but an intermediate auxiliary alignment mark (IM), prepared upfront the stator deposition has to be used. This fact doubles the possible placement error. Values for the overlay-error between yoke and stator for ADI are therefore the sum of the single measurements

$$Ovl(Stator - Yoke) = Ovl(Stator - IM) + Ovl(IM - Yoke) \quad (1)$$

While the AEI-Overlay can be measured directly, in the ADI measurements of Figure 10 one can see the expected enhancement in Overlay for the change from iLine stepper to KrF scanner, however the first AEI measurements were partly out of even the soft specification. Our usual approach, possible in a clean room without high-volume-manufacturing is, to apply a complete lithography rework after first ADI using the obtained corrections parameters. At the moment, these apply only for 0th and 1st order corrections on wafer and shot. After optimization the algorithm for alignment mark detection a feedforward-only correction for lplot#3 was possible, almost attaining the AEI soft spec over the full lot, with only a few chips out of spec, usually at wafer edge. Further analysis of differences between ADI and AEI parameters allowed further enhancement of the resulting overlay, especially taking into account a correction of wafer-scaling bias, induced by sputter-filled alignment marks. Applying feedforward correction parameters from former lots and feedback correction of lot lp#4 itself, the AEI overlay mismatch could be enhanced nearly fully within the hard specification with only little outliers.

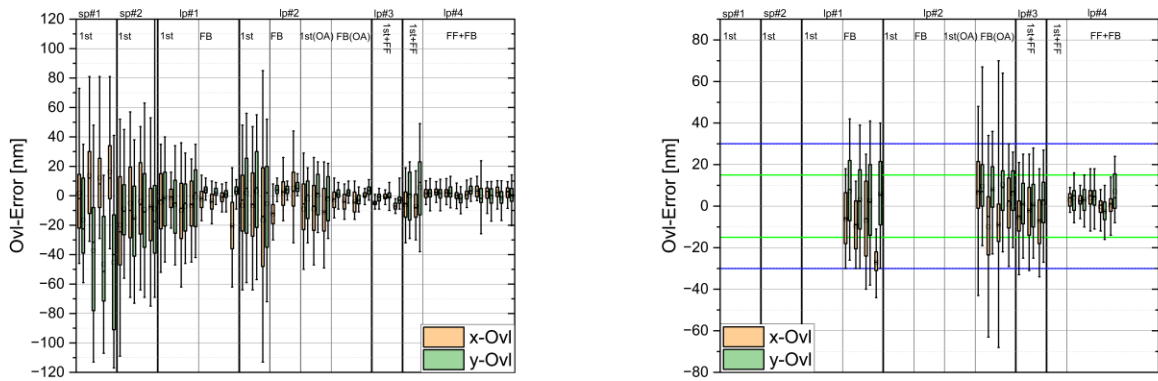


Figure 10: ADI (left) and AEI Overlay (right) for stator-to-yoke alignment of different lots using the iLine design sp#1,2, the 4-finger DUV-design lp#1 and the 5-finger-design lp#2,3,4. Measurements are done after first exposure (1st), rework with overlay corrections (FB) and feedforward overlay correction (FF).

5. SUMMARY AND OUTLOOK

To summarize we presented the processes necessary for the most critical layers of our comb-drive actuator, namely the springs, yoke and stator. For the process development we started with an iLine-compatible design, since KrF-lithography was not available at the beginning of the project. With further progress in the project, more complex designs with smaller feature sizes and higher overlay requirements were developed. Finally, we fully incorporated the KrF-lithography into our process flow for the manufacturing of our MMA device, attaining the hard specifications on CD-uniformity as well as overlay. The project still is in progress and the application of KrF-lithography in our research clean room is still in a loop of continuous learning. We are looking forward to further optimize the results on both CD and overlay, especially with respect to wafer-to-wafer and lot-to-lot stability. Maybe in near future we are going to incorporate enhanced techniques like optical proximity correction of the mask to improve pattern fidelity and ultimately the performance of the holographic device.

ACKNOWLEDGEMENTS

The project REALHOLO has received funding from the European Union's Horizon 2020 research and innovation program under grant agreement No. 101014977. It is an initiative of the Photonics Public Private Partnership. Thanks to the REALHOLO project team for the fruitful discussions supporting the current work and to the IPMS SLM development and fabrication teams for providing the test devices.

REFERENCES

- [1] R. Häussler, S. Reichelt, N. Leister, E. Zschau, R. Missbach, and A. Schwerdtner "Large real-time holographic displays: from prototypes to a consumer product", Proc. SPIE 7237, Stereoscopic Displays and Applications XX, 72370S (2009), <https://doi.org/10.1117/12.805873>
- [2] W. Wu, M. Pivnenko, and C. Daping, "LCOS Spatial Light Modulator for Digital Holography," Photon. Lett. PL 13, 76 (2021).
- [3] REALHOLO project website: <https://realholo.eu>

- [4] M. Nitzsche, P. Dürr, and A. Neudert, "Improved comb drive design for MEMS piston mirror arrays", Proc. SPIE 12434 (2023), MOEMS and Miniaturized Systems XXII, 124340R, <https://doi.org/10.1117/12.2649743>
- [5] P. Dürr, A. Neudert, M. Nitzsche, C. Hohle, H. Stolle, and J. Pleikies, "MEMS piston mirror arrays for computer generated holography", Proc. SPIE 12013, MOEMS and Miniaturized Systems XXI, 1201306 (2022), <https://doi.org/10.1117/12.2608081>
- [6] P. Dürr, A. Neudert, D. Kunze, and M. Friedrichs "MEMS Piston Mirror Arrays with Force-Balanced Single Spring", Proc. SPIE 10931 (2019), MOEMS and Miniaturized Systems XVIII, 1093104, <https://doi.org/10.1117/12.2507007>
- [7] M. Nitzsche, A. Bajpai, P. Dürr, A. Neudert, and A. S. Pranti "First Characterization of Comb Drive Based Micro Mirror Arrays", Proc. MikroSystemTechnik Kongress (2023) in press
- [8] S. Francés González, M. Nitzsche, A. Bajpai, A. S. Pranti, A. Neudert, and P. Dürr "Characterization of MEMS piston mirror arrays with comb drive actuator" Proc. SPIE 12899 (2024), in press
- [9] C. Hohle, S. Döring, M. Friedrichs, A. Gehner, D. Rudloff, M. Schulze, R. Stübner, and D. Trenkler "Challenges of monolithic MEMS-on-CMOS integration for spatial light modulators", Proc. SPIE 11697 MOEMS and Miniaturized Systems XX, 116970V (2021), <https://doi.org/10.1117/12.2583036>
- [10] B. J. Lin, "Can MEMS Take Advantage of Advances in Semiconductor Lithography?" Journal of Micro/Nanolithography, MEMS, and MOEMS 9, 010101 (2010), <https://doi.org/10.1117/1.3372719>
- [11] J-U. Schmidt, M. Friedrichs, and A. Gehner "Amorphous TiAl films for micromirror arrays with stable analog deflection integrated on complementary metal oxide semiconductors", J. Micro/Nanolithography, MEMS, and MOEMS 7, 021012 (2008), <https://doi.org/10.1117/1.2945230>
- [12] S. Döring, P. A. Recknagel, C. Hohle, and P. Dürr, „MEMS-on-CMOS-Integration of Spatial Light Modulator for Holographic MR/AR Applications”, MikroSystemTechnik Kongress 2023, in press
- [13] C. B. Labelle, H. L. Maynard, and J. T. C. Lee "Metal stack etching using a helical resonator plasma", J. Vac. Sci. Technol. B 14, 2574 (1996), <https://doi.org/10.1116/1.588770>
- [14] J. Tonotani, T. Iwamoto, F. Sato, K. Hattori, S. Ohmi, and H. Iwai "Dry etching characteristics of TiN film using Ar/CHF₃, and Ar/Cl₂, and Ar/BCl₃ gas chemistries in an inductively coupled plasma", J. Vac. Sci. Technol. B 21, 2163 (2003) <https://doi.org/10.1116/1.1612517>